Optimization of a microwave resonator cavity to perform Electron Spin Resonance measurements on quantum dots

by

Anat Burger

Submitted to the Department of Physics
in partial fulfillment of the requirements for the degree of

Bachelor of Science in Physics

at the

MASSACHUSETTS INSTITUTE OF TECHNOLOGY
[June 2006]
May 2006

Author .....
Department of Physics
May 12, 2006

Certified by .....
Marc Kastner
Donner Professor of Physics and Department Head
Thesis Supervisor

Accepted by .....
David E. Pritchard
Thesis Coordinator

Optimization of a microwave resonator cavity to perform Electron Spin Resonance measurements on quantum dots

by

Anat Burger

Submitted to the Department of Physics
on May 12, 2006, in partial fulfillment of the
requirements for the degree of
Bachelor of Science in Physics

Abstract

This thesis attempts to improve on an ongoing experiment of detecting electron spin resonance (ESR) on AlGaAs/GaAs lateral quantum dots. The experiment is performed in a 2.5 Tesla magnetic field at temperatures around 100mK. A resonator cavity is used to expose the quantum dot to a perturbational microwave magnetic field pulse that induces electron spin flip transitions. The statistics for measuring the probabilities of these transitions can be improved by increasing the strength and/or the duration of the pulsed magnetic field. The drawback is that both of these improvements lead to thermal heating which diminishes the quantum nature of the dot.

I used electromagnetic field calculations and simulation software to explore different resonant modes, geometries, materials, and methods of excitation and optimize the design of potential new cavities. Two cavities were built specifically to test the TM010 and TE011 cylindrical modes. Although they did not perform as well as was theoretically expected, these cavities provide a better magnetic field magnitude per heating power than the current cavity.

Thesis Supervisor: Marc Kastner
Title: Donner Professor of Physics and Department Head

Acknowledgments

I want to thank Marc Kastner for allowing me to work in his lab and supporting me during my final year at MIT. His positive energy and daily involvement in research is inspiring and motivating.

The work in this thesis could not have been completed without the constant instruction, advice, creativity, and excitement from graduate students Sami Amasha and Kenneth Maclean. They assisted me in all aspects of the design and testing of my project and I would especially like to thank them for their help in the editing of this thesis.

I enjoyed working with the other students in the group including grad students Tamar, Ian, and Juliana and fellow undergrads Emily and Colin.

Finally, I want to thank my parents for their unfailing support throughout my life and for believing in my success as a student.

Contents

List of Figures

List of Tables

Chapter 1

Introduction

1.1 Quantum Dots

A quantum dot is an nanostructure which can confine free electrons to a potential well. This is a physical manifestation of the most fundamental problem in quantum mechanics of a particle in a box. Quantum dots are in many ways analogous to atoms in that the electrons are bound to discrete energy levels and can be observed to individually tunnel on to and off of the dot[1]. There are certain experimental boundaries for effectively studying the discrete quantum properties of an electric current through a macroscopic well. First of all it is necessary that the mean free path of the electrons is large in comparison to the dimensions of the device. It is also necessary that the relevant energy scales are large in comparison to the excitations from thermal energy. These requirements are achieved by confining the dot to very small region and performing the experiment at extremely low temperatures.

In order for the number of electrons on the dot to be well defined two criteria must be met. First, the charging energy to add one electron to the dot must be large compared to the thermal energy, $k_B T$. This charging energy is $E_C = \frac{e^2}{C}$ where C is the capacitance between the dot and the surrounding leads. This criteria can achieved by making the dot small and performing the experiment at low temperatures. For a dot of radius 200nm, the charging energy $E_C \simeq 1meV$ which is much larger than the thermal energy at 100K which is .0086meV. The second requirement is that the flux

of current due to tunneling must be slow enough to observe discrete electrons. The time scale of the tunneling is $\Delta t = R_t C$ where R_t is the tunnel barrier resistance. The uncertainty principle requires that the lifetime broadening in the energy levels, $\Delta E \geq h/\Delta t = h/R_t C$. If we require that the charging energy must be larger than the broadening ΔE that means that $R_t \geq \frac{h}{C}\frac{C}{e^2} = \frac{h}{e^2}$ which happens to be the resistance quantum of 25.813 kΩ[2].

There are several advantages to creating a quantum dot that is confined to two dimensions. The energy spacings between the quantum levels in a two dimensional dot of length L is given by

$$\Delta E = \frac{\hbar^2 \pi}{mL^2} \tag{1.1}$$

which is obtained by simply inverting the 2D energy density of states. Most notably ΔE is independent of the number of electrons on the dot. In 1D systems $\Delta E \propto N$ and for 3D, $\Delta E \propto N^{1/3}$. Quantum dots are typically formed in semiconductors such as GaAs where the effective mass of the electrons is very small, $m* = 0.067 m_e$, so that ΔE for a 100nm dot in 2D is 0.03 meV. This is significantly larger than the thermal energy of a dilution refrigerator temperature of 100 mK $\approx$ 0.0086 meV. For a 3D dot the dimensions would need to be as small as 5 nm to be able to distinguish individual energy levels[2].

One system commonly studied is the semiconductor lateral quantum dot. A two dimensional electron gas or 2DEG is formed at the planar interface between two semiconductors, typically GaAs and $Al_xGa_{1-x}As$. The electrons are restricted from moving perpendicular to this interface because of a narrow potential well formed from the conduction band offset between the two semiconductors and by the attractive potential due to the positively charged n-doped AlGaAs. The doped Si atoms are placed in a layer that is clear of the interface when the material is made using molecular beam epitaxy (MBE) techniques. This allows the scattering length of the electrons to be as large as half a millimeter. The shape of the dot can be defined by placing metal gates on top of the GaAs surface that can be negatively biased to deplete the

electron gas directly underneath.

Quantum dots are interesting because they can be studied as artificial atoms. Source and drain leads can be attached to the dot and gate voltage can be applied to conduct a current, creating what is referred to as a single electron transistor. Figure (1-1) shows a potential well with source and drain tunnel barriers. Figure (1-2) illustrates the parameters for observing a single electron current through a quantum dot. The voltage between the source and drain, V_{sd} can be adjusted as can the electrostatic potential of the gate V_g. Conduction through the dot can only occur when there is an available state at $\mu(N)$ between the chemical potentials of the source and drain, μ_{left} and μ_{right} At very low temperatures these side walls are effectively filled up to the fermi energy. In what is called the linear transport regime, a small voltage is applied between the source and the drain and periodic peaks in the conductance occur as the gate voltage is swept, corresponding to single electrons piling on to and off of the newly available quantum states. If $\mu_{left} \approx \mu_{right}$ lies in between the gap formed by the charging energy, $E_C = \frac{e^2}{C}$ then there will be no conductance through the dot. In this regime the dot is said to be demonstrating *Coulomb blockade.* If the thermal energy $k_B T$ is sufficiently smaller than the spacings between the energy levels, the peaks in conductance will be sharp and decrease linearly with increasing temperature. As the dot warms up the peaks broaden and eventually the individual charges become indiscernible.

V_g

1.2 Electron Spin Resonance

Quantum dots make a exciting candidate for the future creation of a quantum computer. This is because in a magnetic field they can form a very simple, easily manipulated two state system consisting of a spin-down excited state and a spin-up ground state. This Zeeman energy splitting is proportional to the magnitude of the magnetic field. The energy of an electron with a magnetic moment $\vec{\mu}$ in a magnetic field $\vec{B}$ is

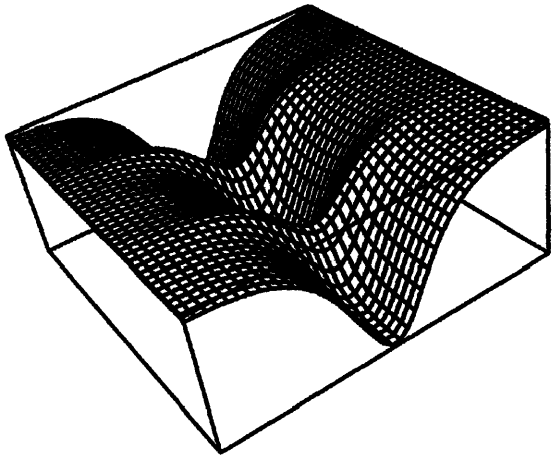

Figure 1-1: Illustration of a quantum dot potential well with source and drain tunneling barriers

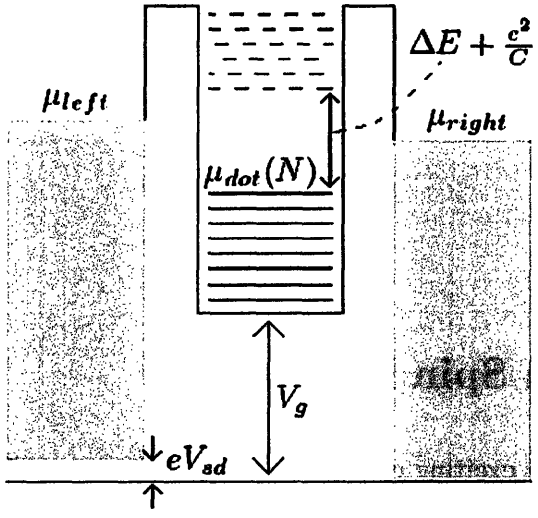

Figure 1-2: Mechanism for observing coulomb blockade.

given by

$$U = -\vec{\mu} \cdot \vec{B} = \pm\frac{1}{2} g\mu_B B \tag{1.2}$$

where g is the gyromagnetic moment of the electron and $\mu_B = \frac{e\hbar}{2m_e}$ is the Bohr magneton. This means that the energy splitting of the transition from spin down to spin up is $\Delta E_Z = g\mu_B B$[3]. For our experiment $\Delta E_z \approx 55\mu eV$ which corresponds to a microwave frequency of 13 GHz. For a thermal energy of around $10\mu eV$ electrons will most probably initially be aligned with the magnetic field in the ground state.

There are two time constants associated with all magnetic resonance experiments. The first is T_1, the spin-lattice relaxation time. T_1 is defined as $1/P_\downarrow$ where $P_\downarrow$ is the probability of a relaxation transition from the excited state to the ground state. If P_e is the probability of finding an electron in the excited state and P_g is the probability of finding it in the ground state, the following first-order kinetics must be followed:

$$\dot{P}_e = P_\uparrow P_g - P_\downarrow P_e$$

Conserving probability $P_e + P_g = 1$ to eliminate P_g:

$$\dot{P}_e = P_\uparrow - (P_\uparrow + P_\downarrow) P_e$$

Solving the differential equation and using the limit that $P_\downarrow \gg P_\uparrow$ gives the following result:

$$P_e \simeq \frac{P_\uparrow}{P_\downarrow}(1 - e^{-P_\downarrow t})$$

This means that on a plot of P_e over time, if a plus is started at time t = 0, it will take a time T_1 for P_e to rise to 1/e of its final value of $\frac{P_\uparrow}{P_\downarrow}$ (See Fig. 1-3). T_1 is a measurement of the ability of the excited state electron to dissipate energy[3]. T_1 can be found experimentally by positioning the excited state but not the ground state in between the source and drain potentials. The tunneling rates are determined by

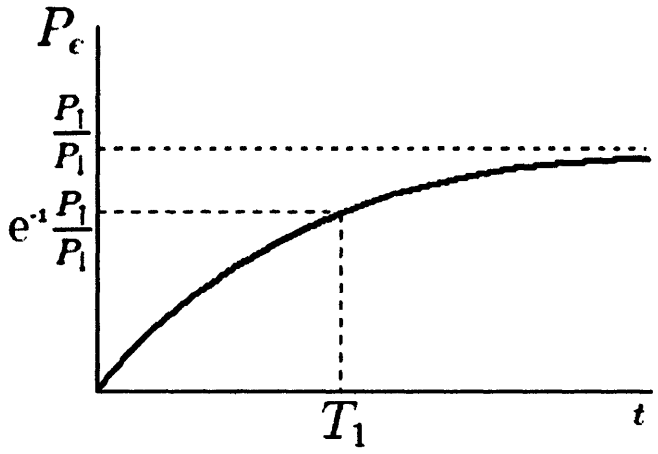

Figure 1-3: Probability of finding an electron in the excited state over time

steady state measurements. Varying pulse widths are applied and the average current is measured. The longer the field can be pulsed, the more accurate value for T_1 can be determined. For our system T_1 is quite slow, 50ms, so the applied field can cause significant heating. On the current experimental setup 1mW of power in the cavity corresponds to 2 milligauss of field and raises the cavity temperature from 120 mK to 350 mK.

The second time constant, T_2 is called the spin phase decoherence time. It is a measurement of the time it takes for the relative phase between the spin up states and spin down states to change. Usually $T_2 < T_1$ so obeying the uncertainty principle, T_2 is mostly responsible for the broadening in energy and therefore the current through the dot as a function of frequency of the field. Right at resonance the probabilities of finding the electron in the spin up or spin down state will oscillate with a frequency that is dependent proportional to the strength of the microwave magnetic field. This is called a Rabi oscillation. In is difficult to obtain accurate data from ESR in the limit that ν_{Rabi} is smaller than the linewidth of the spin-flip transition, which is approximately $1/T_2$. Our experiment operates in this weak field limit, where the spin flip probabilities, obeying Fermi's golden rule, are proportional to the microwave field magnitude squared. Unfortunately the power which causes heat in the cavity walls will also be proportional to the field magnitude squared.

The challenge for this project is to maximize the magnetic field applied to the dot for a given power heating the cavity.

Chapter 2

Theory

2.1 Q factor

ESR experiments require an oscillating magnetic field at microwave frequencies. It is not feasible to use a solenoid or any other elements requiring wires at these frequencies because the skin effect creates a high effective resistance and too much energy would be lost to radiation [4]. The solution is to use a microwave resonator cavity. This cavity is simply a box with metallic walls that has dimensions comparable to the wavelength needed. The cavity is excited by a coaxial cable carrying signals from a network analyzer. Currents in the walls set up standing waves that form resonant modes at certain frequencies.

The fields in a cavity are similar to what might be found in a waveguide, except that in a waveguide the transverse electric and transverse magnetic fields reach a maximum at the same position. Thus there is a nonzero time averaged pointing vector (a factor of $E \times H$)that defines energy flow. In a cavity there is only energy storage and dissipation, so the electric and magnetic fields form a maximum at a quarter wavelength away from each other. They are also 90° out of time phase with each other.

Figure [2.1] shows several of the most common transverse magnetic and transverse electric modes. The fields obey a "space quadrature" right hand rule geometry. As always there are no electric fields tangent to and no magnetic fields perpendicular to

the surface of the cavity. In transverse magnetic modes the magnetic field encloses an electric field that "travels" back and forth through the cavity. In transverse electric modes the electric field either encloses the magnetic field or terminates on the induced surface charge.

The indices that describe the TE_{nml} and TM_{nml} modes refer to the number of half wavelength variations in the radial, axial, and longitudinal directions. The resonant frequency depends only on the geometric parameters of the cavity which are l, the hight of the cavity and d the diameter of the cavity[5]:

$$f_{nml} = \frac{c}{2\pi\sqrt{\mu_r \epsilon_r}}\sqrt{(\frac{p'_{nm}}{a})^2 + (\frac{l\pi}{d})^2} \tag{2.1}$$

A cavity resonator behaves like a damped harmonic oscillation and can be described as a series LRC circuit. The complex impedance is as follows:

$$Z_{in} = R + j\omega L - j\frac{1}{\omega C} \tag{2.2}$$

The power lost due to resistance in the walls of the cavity is

$$P_{loss} = \frac{1}{2}|I|^2 R \tag{2.3}$$

The stored magnetic energy is

$$W_m = \frac{1}{4}|I|^2 L \tag{2.4}$$

The stored electric energy is

$$W_e = \frac{1}{4}|I|^2 \frac{1}{\omega^2 C} \tag{2.5}$$

The quality factor Q is a measure of the decay of the oscillation of a cavity after it is excited at resonance. The value of Q is the number of cycles in the time taken for the amplitude to drop to 1/e of its initial value. Another definition of Q is as follows:

$$Q = \frac{\omega(W_m + W_e)}{P_{loss}} \tag{2.6}$$

Where W_m is the total magnetic energy and W_e is the total electric energy over

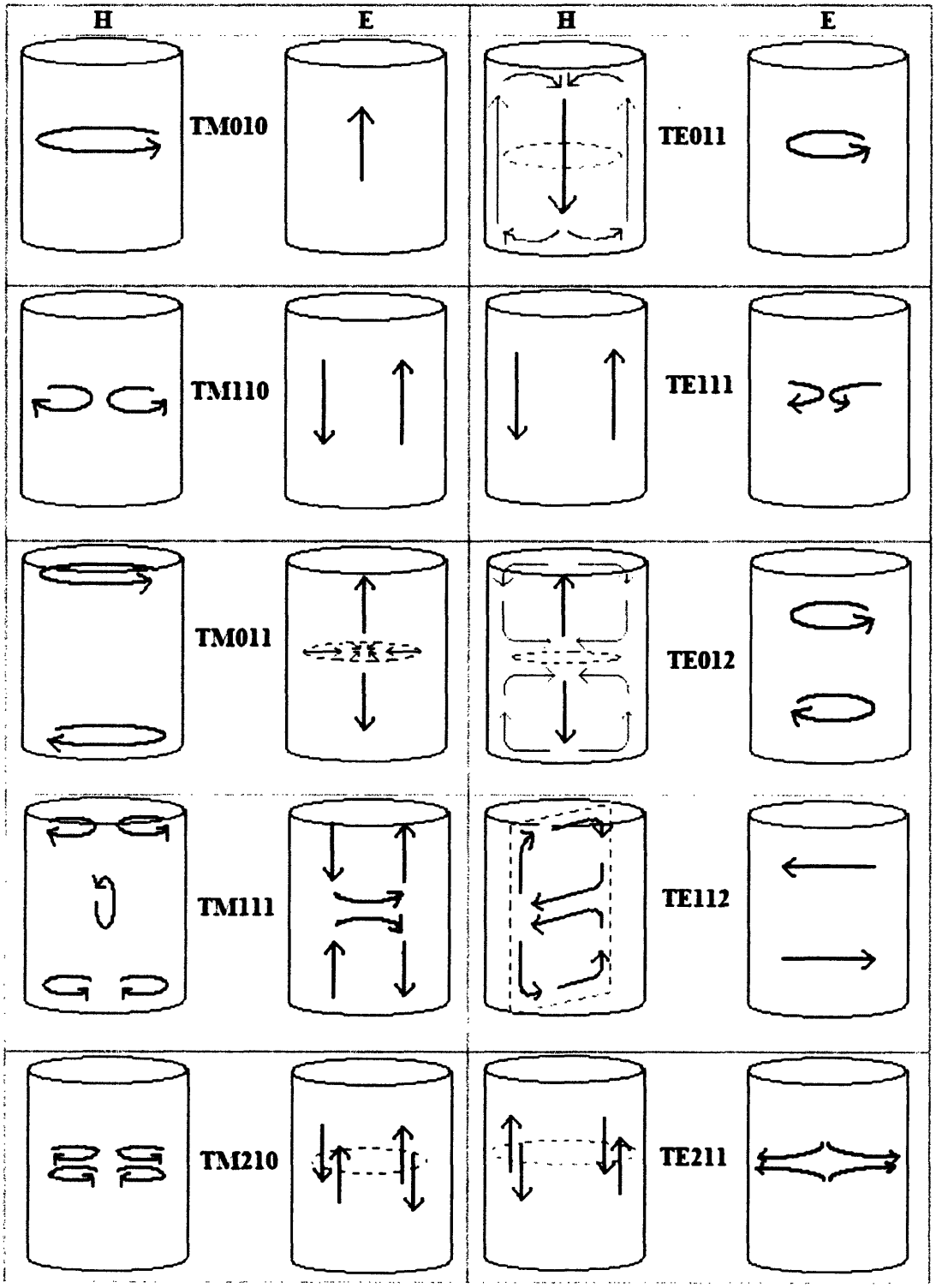

Figure 2-1: **Mode Chart** This table shows the lowest order TE and TM modes. The magnetic field (left) is shown in blue and the electric field (right) is shown in red for each mode. Both are shown at their maximums, which would be 90^0 out of phase in time.

one period.

At resonance, the magnetic and electric energy stored in the cavity is equal and by setting equations (2.3) and (2.4) equal you obtain

$$\omega_0 = \frac{1}{\sqrt{LC}} \tag{2.7}$$

and inserting into equation (2.5),

$$Q = \frac{\omega_0 L}{R} = \frac{1}{\omega_0 RC} \tag{2.8}$$

In order to measure the Q of a cavity it is sometimes convenient to excite the cavity at a ramp of frequencies and to measure the reflected power that returns from the cavity. When the cavity is excited on resonance, power will be absorbed and there will be a dip in the reflection spectrum. To look slightly off resonance let's let $\omega = \omega_0 + \Delta\omega$. The complex impedance takes the form

$$Z_{in} = R + j\omega L(\frac{\omega^2 - \omega_0^2}{\omega^2}) \tag{2.9}$$

To simplify this $\omega^2 - \omega_0^2 = (\omega - \omega_0)(\omega + \omega_0) = \delta\omega(2\omega - \Delta\omega) \simeq 2\omega\Delta\omega$ for small $\Delta\omega$. Plugging back into equation (8) gives

$$Z_{in} = R + 2jL\Delta\omega \simeq R + j\frac{2RQ\Delta\omega}{\omega_0} \tag{2.10}$$

The power transmitted into a cavity is usually reflected back and attenuated slightly due to the current losses in the walls.

$$P_{in} = P_{loss} + 2j\omega(W_m - W_e) \tag{2.11}$$

At resonance all of the power lingers in the cavity, $P_{in} = P_{loss}$, and the complex impedance is all real.

$$Z_{in} = \frac{2P_{in}}{|I|^2} = \frac{2P_{loss}}{|I|^2} = R \tag{2.12}$$

Squaring both sides of equation (9) and combining with (10)

$$|Z_{in}|^2 = R^2 = |R + j\frac{2RQ\Delta\omega}{\omega_0}|^2 \tag{2.13}$$

Which gives us the result that the Q is the inverse bandwidth of the dip in reflection from the cavity at resonance.

$$Q = \frac{\omega_0}{2\Delta\omega} \tag{2.14}$$

2.1.1 Losses at a good conductor

Equation (2.3) can be rewritten more practically by using a version of Ampere's Law,[1]

$$P_{loss} = \frac{R_s}{2}\int |H_{tan}|^2 ds \tag{2.15}$$

where H_{tan} is the magnitude of the magnetic field that is tangential to the surface of the cavity. The surface resistance is given by

$$R_s = \sqrt{\frac{\omega\mu}{2\sigma}} = \frac{1}{\sigma\delta_s} = \frac{j\omega\mu}{\gamma} \tag{2.16}$$

where $\gamma = \alpha + j\beta$ is the complex propagation constant. In the lossless case

$$\gamma = jk = j\omega\sqrt{\mu\epsilon}$$

and $R_s = \sqrt{\frac{\mu}{\epsilon}} = \eta = 337Omega$ which is the impedance of free space. In a conductor the skin depth is the inverse of the attenuation constant such that

$$\delta_s = \frac{1}{\alpha} = \sqrt{\frac{2}{\omega\mu\sigma}}$$

The skin depth is a measure of the penetration of a reflected electric field in a material. (See Chapter 4)

[1]For a precise derivation please see p. 38 of Ref. [5]

2.2 g factor

Rearranging equations 2.4-2.6 there are several equivalent expressions for the total energy of a cavity at resonance:

$$W_{tot} = \frac{Q \cdot P_{loss}}{\omega} = \frac{\epsilon}{2}\int |\vec{E}|^2 dV = \frac{\mu}{2}\int |\vec{H}|^2 dV \tag{2.17}$$

In traditional ESR experiments the sample would be loaded into the resonator cavity, but this cannot be done with a quantum dot because the leads to the device cannot be exposed to electromagnetic fields. As an alternative, a small hole in the cavity allows for magnetic flux to pass through the small area of the dot and nowhere else. When analyzing the electromagnetic fields it will be convenient to scale the total magnetic field in the cavity by the magnitude of the magnetic field at the point of interest, directly on the surface of the cavity positioned at the hole, halfway up the hight.

$$\vec{H} = H_{hole} \cdot f(x, y, z) \tag{2.18}$$

A variable g, the geometric factor, is used to represent the volume integral of the dimensionless field function.

$$g = \int |f(x, y, z)|^2 dV \tag{2.19}$$

Substituting this factor into equation (2.17) gives

$$\frac{Q \cdot P_{loss}}{\omega} = \frac{\mu g}{2}|H_{hole}|^2 \tag{2.20}$$

In the case of our experiment it is desirable to maximize the magnetic field strength at the hole per total power transmitted into the cavity. At resonance this power is entirely converted into heat creating a significant thermal load in the cryostat.

$$\frac{|H_{hole}|^2}{P_{loss}} = \frac{2Q}{\mu\omega g} \tag{2.21}$$

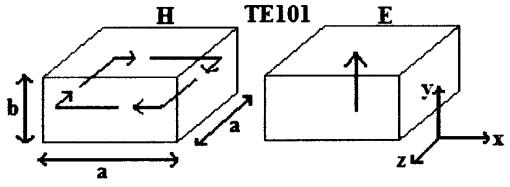

Figure 2-2: **TE011 mode in a rectangular cavity** In our case a = 1.58 cm, b = 0.79 cm, f_0 = 13.6 GHz

In order to maximize this ratio it will be necessary to maximize Q by minimizing the surface resistivity R_s (See chapter 4) and to minimize g by exploring different mode geometries (See below).

2.3 TE011 rectangular mode

We begin with an analysis of the fields in the current rectangular cavity. The TE011 mode (See Figure 2-2) is the lowest order mode in this cavity. The electric and magnetic fields of this mode are given by the following:

$$E_y = E_0 sin\frac{\pi x}{a} sin\frac{\pi z}{b} \tag{2.22}$$

$$H_x = \frac{-jE_0}{Z_{TE}} sin\frac{\pi x}{a} cos\frac{\pi z}{b} \tag{2.23}$$

$$H_z = \frac{j\pi E_0}{k\eta a} cos\frac{\pi x}{a} sin\frac{\pi z}{b} \tag{2.24}$$

where $Z_{TE} = \frac{k\eta}{\beta}$ is the wave impedance, η is the intrinsic impedance, $k = \frac{2\pi f}{c}$ is the wave number, $\beta = \sqrt{k^2 - k_c^2}$ is the propagation constant, $k_c = \frac{\pi}{a}$ is the cutoff wave number. At resonance the stored energy in the cavity is twice the stored electric energy:

$$W = 2W_e = \frac{\epsilon}{2}\int |\vec{E}|^2 dV = \frac{\epsilon a^2 b}{8} E_0^2 = 2W_m = \frac{\mu_0}{2} H_{hole}^2 g \tag{2.25}$$

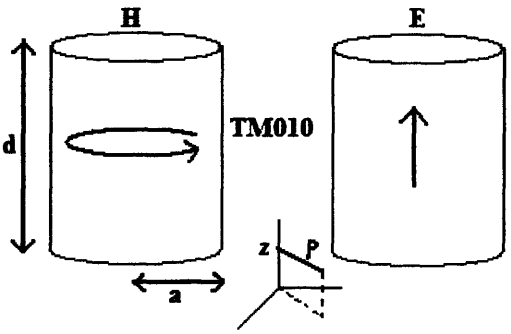

Figure 2-3: **TE010 mode in a cylindrical cavity** In our case a = 0.81 cm, d = 0.81 cm, f_0 = 14.1 GHz

which is equal to twice the stored magnetic field energy. From equation (2.18) this value can be scaled by the value of the useful magnetic field at the hole, which has a value of $\vec{H_{hole}} = -\frac{E_0}{Z_{TE}}\hat{x}$. Squaring this gives $|H_{hole}|^2 = \frac{E_0^2}{Z_{TE}^2}$ Rearranging equation (2.20) and plugging in the values for our resonator, one can find a value for the g factor:

$$g = \frac{W}{\mu_0 H_{hole}^2} = \frac{a^2 b}{4}\frac{\epsilon Z_{TE}^2}{\mu} = \frac{a^2 b}{4}\frac{k^2}{\beta^2} = \frac{(0.0158m)^2(0.0078m)(285m^{-1})^2}{4(204m^{-1})^2} = 1.9cm^3$$

This is all that is needed to calculate the desired ratio. Using the experimental result that Q = 2800,

$$\frac{H_{hole}^2}{Power} = \frac{2Q}{g\omega} = \frac{2(2800)}{(1.9 \times 10^{-6}m^3)(2\pi \times 13.6 \times 10^9 s^{-1})} = 0.0086\frac{s}{m^3}$$

2.4 TM010 mode

We choose to explore modes in cylindrical cavities for the reasons stated in chapter 4. The TM010 mode was of particular interest for several reasons. It is the lowest order mode for cylindrical cavities which means that it can be excited in a cavity with the smallest dimensions for our desired resonant frequency. This is because the wavelength of the mode scales with the dimensions of the cavity, thus lower resonant frequencies mean larger cavities. In order to excite a higher order mode it would be

necessary to increase the scale of the cavity to lower the frequency to the desired range. We wish to minimize the size of the cavity if possible because we are limited for space in the cryostat.

Another reason for choosing this mode is because it sets up a maximum of the magnetic field and minimum of the electric field along the walls of the cylinder. This is precisely the desired configuration. This mode is referred to by experimentalists as the "Whispering Gallery" mode because it is analogous to round rooms built with the acoustical property that one can talk to someone along the wall of the room by whispering (See Figure 3-1).

The electric and magnetic fields for this cavity are given by the following, where J_0' is the derivative of the first Bessel function and $p_{01} = 2.4048$ is the first root of J_0.

$$H_\phi = \frac{jkaE_0}{\eta(p_{01})} J_{01}'(\frac{p_{01}\rho}{a}) \tag{2.26}$$

$$E_z = E_0 J_{01}(\frac{p_{01}\rho}{a}) \tag{2.27}$$

$$W = 2We = \frac{\epsilon}{2}\int |\vec{E}|^2 dV = \frac{\epsilon}{2} E_0^2 d(2\pi) \int_{\rho=0}^{a} J_{01}^2(\frac{p_{01}\rho}{a})\rho d\rho$$

$$= \frac{\epsilon\pi a^2 d}{2} E_0^2 J_0'(p_01)^2 = \frac{\mu_0 a d\pi(p_{01})}{2k} |H_{hole}|^2$$

[2]

using the substitution that $H_{hole} = \frac{kaE_0 J_0'(p_{01})}{\eta(p_{01})}$ Rearranging the above equation to solve for g:

---

[2]Using the identity:

$$\int_0^x J_0^2(kx)xdx = \frac{x^2}{2}(J_0')^2(kx) + J_0^2(kx)$$

let's let $x = \frac{\rho}{a}$ and $dx = \frac{1}{a}d\rho$

$$a^2 \int_0^x J_0^2(p_{01}x)xdx \,|_{x=1}\,|_{k=p_{01}} = \frac{a^2x^2}{2}(J_0')^2(kx) + (J_0)^2(kx) = \frac{a^2}{2}(J_0')^2(p_{01})$$

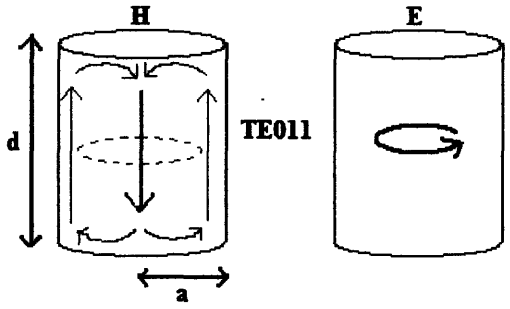

Figure 2-4: **TE011 mode in a cylindrical cavity** In our case a = 1.33 cm, d = 1.88 a, f_0 = 15.1 GHz and $k = 295m^{-1}$

$$g = \frac{W}{\mu_0 H_{hole}^2} = \frac{ad\pi(p_{01})}{2k} = \frac{(0.0081m)^2\pi(2.405)}{2(295m^{-1})} = 0.84cm^3$$

$$\frac{H_{hole}^2}{Power} = \frac{2Q}{g\omega} = \frac{2(3600)}{(8.4 \times 10^{-7}m^3)2\pi(14.1 \times 10^9 s^{-1})} = 0.097\frac{s}{m^3}$$

2.5 TE011 mode

We chose to explore this mode because it is most frequently used in ESR experiments. Typically a sample is loaded directly in the center of the cavity, where the magnetic field is a maximum. We cannot use this portion of the field for the reasons stated above, however, in our experiment it is convenient that there is a magnetic field along the walls of the cavity. Another reason why this mode is useful for ESR is that the Q of this cavity is theoretically three to four times as large as the other modes. This is because there is no build up of charge and no current flow between the body and lids of the cavity. The currents that create this mode simply swirl back and forth along the circumference of the cylinder. A new cavity was needed to test this cavity because it required a different optimization for the aspect ratio,as explained in Chapter 3, and it needed to be scaled to a larger size in order to resonate at the proper frequency.

The electric and magnetic fields for this cavity are given by the following, where

J_0 is the first Bessel function and $p'_{01} = 3.832$ is its first root.

$$H_z = H_0 J_0(\frac{p'_{01}\rho}{a}) sin\frac{\pi z}{d} \tag{2.28}$$

$$H_\rho = \frac{\beta a H_0}{p'_{01}} J'_0(\frac{p'_{01}\rho}{a}) cos\frac{\pi z}{d} \tag{2.29}$$

$$E_\phi = \frac{jk\eta a H_0}{p'_{01}} J'_{01}(\frac{p'_{01}\rho}{a}) sin\frac{\pi z}{d} \tag{2.30}$$

As before we can calculate the total magnetic field energy by integrating the electric field over the volume. A Bessel function identity is used to solve the integral.

$$W = 2W_e = \frac{\epsilon}{2}\int |\vec{E}|^2 dV = \frac{\epsilon}{2}\frac{d}{2}(2\pi)\int_0^a |E_\phi|^2 \rho d\rho = \frac{\epsilon d\pi k^2\eta^2 a^2 H_0^2}{(p_{01})'^2}\int_0^a (J_0)^2(\frac{p'_{01}\rho}{a})\rho d\rho$$

$$= \frac{\epsilon d\pi k^2\eta^2 a^4 H_0^2}{8(p_{01})'^2}(J_{01})^2(p'_{01}) = \frac{\mu_0}{2}H_{hole}^2 g$$

The value of the magnetic field at the hole is given by $\vec{H}_{hole} = H_0 J_0(p'_{01})\hat{z}$. Squaring this gives $|H_{hole}|^2 = H_0^2 J_0^2(p'_{01})$. Rearranging the above equation to solve for g gives

$$g = \frac{W}{\mu_0 H_{hole}^2} = \frac{k^2 a^4 d\pi}{8(p_{01})^2} = \frac{(314m^{-1})^2(0.0133m)^5(1.88)\pi}{8(3.832)^2} = 2.06cm^3$$

$$\frac{H_{hole}^2}{Power} = \frac{2Q}{g\omega} = \frac{2(4600)}{2\pi(15.08\times 10^9 s^{-1})(2.06\times 10^{-6}m^3)} = 0.0471\frac{s}{m^3}$$

2.6 Results

This field analysis shows that for the particular cavities that we built, the TM010 mode shows a similar magnetic field magnitude squared per power dissipated compared to the current rectangular cavity. The TE011 mode has a smaller ratio, mainly

because the field at the edge is not a maximum and the dimensions of the cavity are larger.

Chapter 3

HFSS design

Ansoft High Frequency Structure Simulator (HFSS) is an interactive 3D software package for calculating electromagnetic behavior of a structure. It is used by engineers for the design of microwave and RF electronics. A user must first draw a 3D model of a device, specify the materials used with a precise value of the conductivity, and indicate the method of excitation. The software then calculates the field solutions, resonant frequencies, and quality factor of the structure. The user can then visualize the fields animated over an entire period or plot data to analyze a wide range of parameters. In this thesis HFSS was used to model the cavities and explore the possible modes before spending the time and money to build them.

3.1 Data

The HFSS software was used initially to study the possible modes to be used for ESR. The reasons why we chose the TM010 and TE011 modes were stated in Chapter 2. Fig 5-2 and 5-3 show the magnitudes of the electric and magnetic fields along the normalized distance of a line that extends from the center of the cavity to the circumference and out a small hole half way up the height.

The next two sets of graphs were made by doing individual simulations on cavities with different aspect ratios. In the design of the TM010 mode, 8 cavities were simulated with varying aspect ratios but constant volume. The magnetic field at the

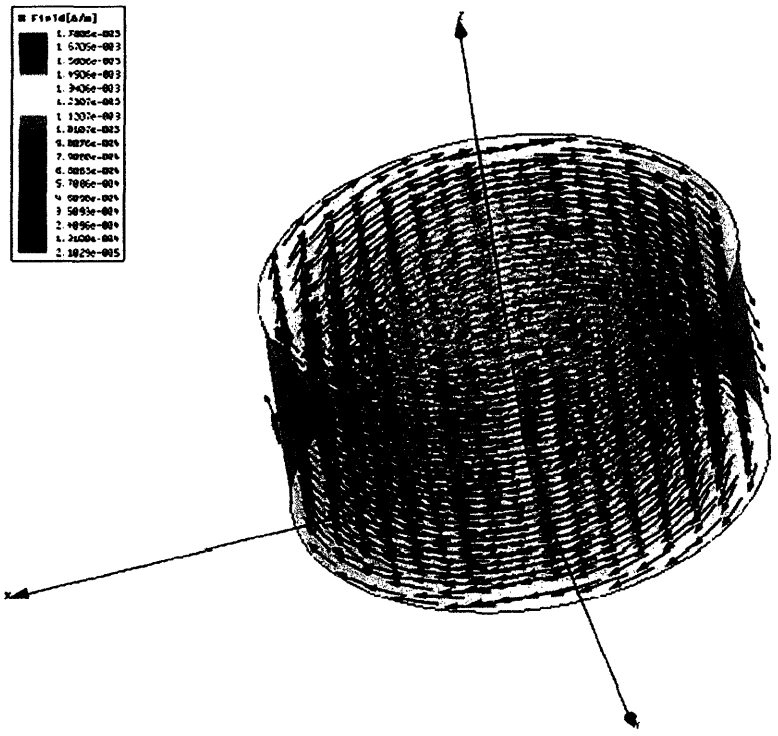

Figure 3-1: **Mode in HFSS simulation** Magnetic field vector illustration of the TM010 mode in a cylindrical cavity

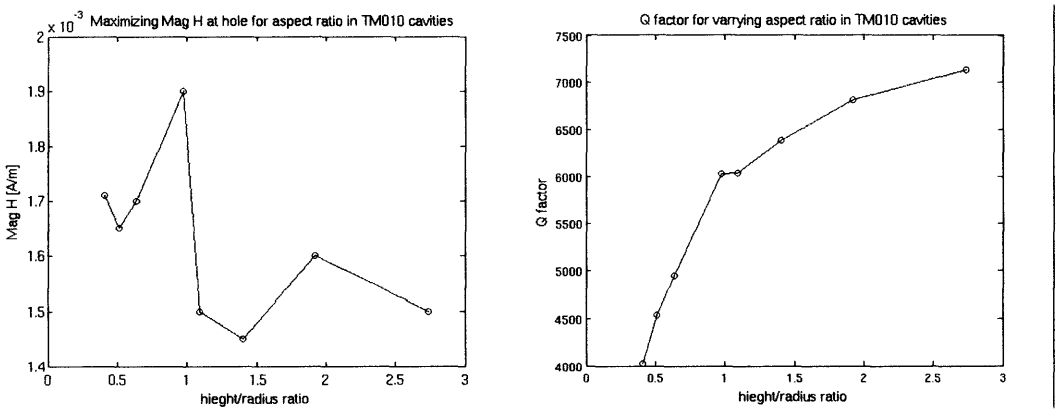

Figure 3-2: Difference in Q factor after tightening on screws

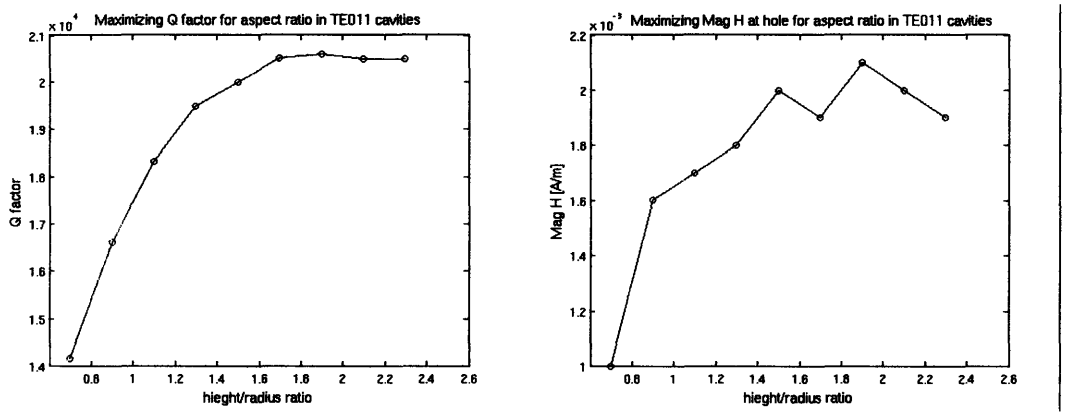

Figure 3-3: Difference in Q factor after tightening on screws

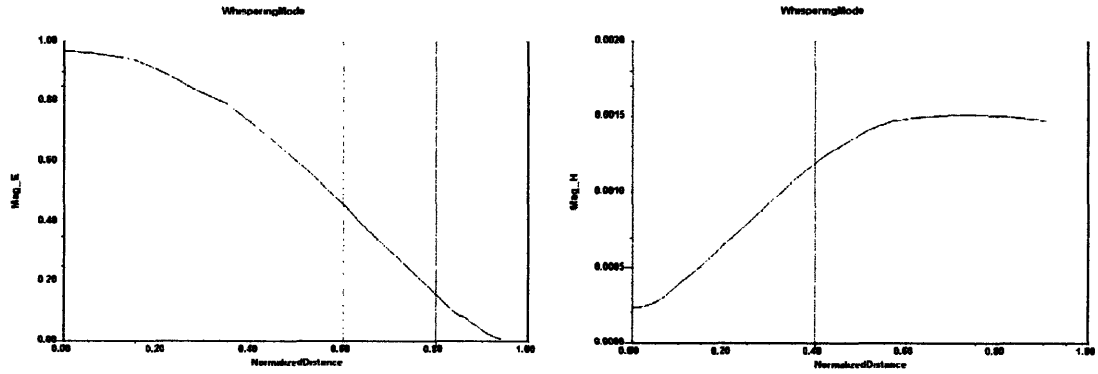

Figure 3-4: Electric field (left) and magnetic field (right) magnitude for the TM010 mode in Cavity A

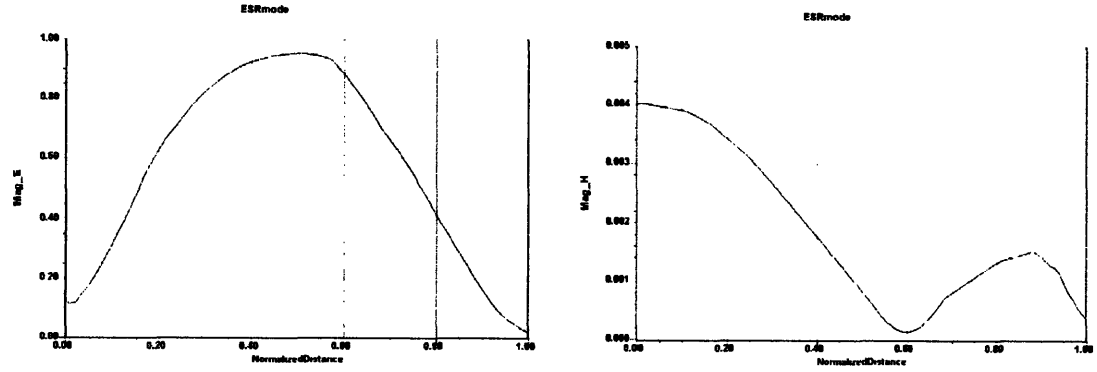

Figure 3-5: Electric field (left) and magnetic field (right) magnitude for the TE011 mode in Cavity B

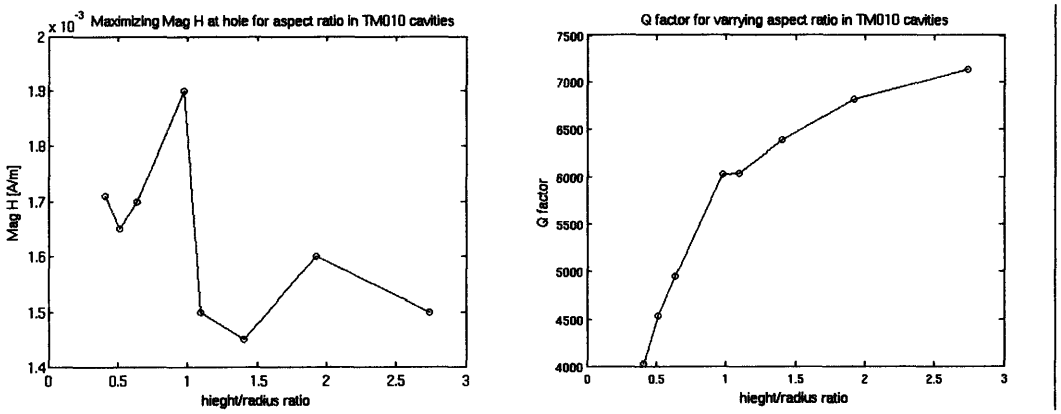

Figure 3-6: Optimization of aspect ratio for TM010 mode

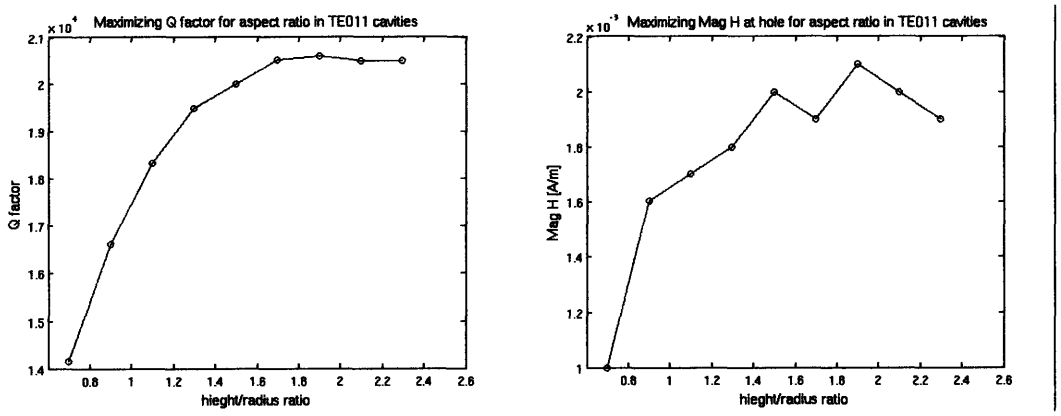

Figure 3-7: Optimization of aspect ratio for TE011 mode

edge and the Q factor for these cavities is plotted in Fig 3.4. The best aspect height to radius ratio was around 1. The final cavity (Cavity A)had a radius and height of 0.32".

In the design of the TE011 mode the following equation was used:

$$f_0 = \frac{c}{\sqrt{\mu_r \epsilon_r}} [\frac{\sqrt{1 + (\frac{2l}{1.64a})^2}}{2l}] \tag{3.1}$$

which is adapted from equation 2.1, where l is the height and a is the radius of the cavity. This formula specified the dimensions for 9 cavities with varying aspect ratios given the same resonant frequency of 15GHz. The magnetic field at the edge and the Q factor for these cavities is plotted in Fig 3.5. The best aspect ratio was 1.9, which meant a height of 2.5cm and a radius of 1.3cm (Cavity B).

Chapter 4

Design and Construction

To begin the design process I first researched the work of 8-10 groups that used high Q cavities, some at low temperatures. All of them used cylindrical cavities. Most of them were built out of Oxygen Free High Conductivity (OFHC) Copper. Most were plated with gold to prevent oxidation.

4.1 Material used

In deciding on the proper material for the cavity we were interested in finding a good conductor to allow for low resistance currents in the walls that could be polished to a smooth surface to minimize scattering losses from the reflections of the electromagnetic waves. As mentioned in section 2.1 the surface resistance of currents in a conductor exposed to electromagnetic fields is given by the following,

$$R_s = \sqrt{\frac{\omega\mu}{2\sigma}} \tag{4.1}$$

where ω is the frequency of the fields, μ is the permeability, and σ is the conductivity. Since the Q of a cavity scales like the inverse of the surface resistance (See Eq. 2.6) it can be inferred that the Q of a cavity is proportional to $\sqrt{\sigma}$. For this reason it is necessary to use a high conductivity material for the plating of the cavity. Although silver and copper have very high electrical conductivities, they are undesir-

Table 4.1: Electrical conductivity metals at 300K [10^7 S/m][6]

Al	3.65
Cu	5.88
Cr	0.78
Au	4.55
Ag	6.21
Ni	1.42

able because they oxidize when exposed to air. The best material is gold, which does not oxidize, can be plated easily using a Ni adhesion layer, and can be polished to a very smooth surface.

It can also be assumed that since the conductivity of a material increases with decreasing temperature, the Q of the cavity should also increase. The conductivity of gold increases 100 fold[1], from 4.5×10^7 [S/m] at 300K to 440×10^7 [S/m] at 10K. This means that the Q should theoretically increase by 10 times it's value as it is cooled to liquid helium temperatures. As shown in the next chapter, we were unable to achieve such results.

The skin depth is a measure of the penetration of a reflected electric field in a material. At one skin depth the conductivity is reduced to 37% of what it is at the surface. At $2\delta_s$ it is 13.5% and at $5\delta_s$ it is 0.7%. That is why microwave engineers recommend that all plating be at least 5 skin depths thick. For our purposes the skin depth for gold is 0.64μm at room temperature and 0.06μm at 1K. This was not an issue for us because the plating was between 50 and 130μm thick.

4.2 Hole

As mentioned earlier, in our experiment ESR is performed by drilling a small hole in the side of the resonator cavity and exposing the quantum dot, but not the surrounding leads to the dot, to a small amount of magnetic flux. It is very important that the hole be drilled through a very thin piece of metal as to limit attenuation

[1]The residual resistivity ratio (RRR) of gold is approximately 100

of the field strength. In the rectangular cavity this is achieved by making an entire wall of the cavity out of thin copper foil and soldering the edges. This is undesirable because the seams of the cavity are imperfect and can lead to losses. Also to create good contact the device must be mounted right up against the foil. The geometry of a cylindrical cavity allows for only a narrow portion of the edge to be shaved away, without attaching a separate wall. This also allows for the option of decoupling the hole that narrows the flux from the cavity.

4.3 Lids

One concern with the rectangular cavity was that when the side flange was screwed on, contact was being made primarily at the location of the screws and not around the rim of the cavity. In order to eliminate this problem I designed a narrow, elevated rim that would create a tight contact exactly where it was needed. At first we designed a series of six screws evenly spaced around top and bottom lid. After testing the cavity (see chapter 5) we decided to drill holes straight through the body of the cavity to create the tightest clamp around the top and bottom.

4.4 Coupling

In order to perfectly couple the cavity a coaxial cable with an antennae at the end must be placed inside the cavity at the precise maximum of either the electric or magnetic field one wishes to excite. For electric coupling a small portion (0.5 cm) of the cable is striped. The TM010 mode is excited by electric coupling. For magnetic coupling the striped cable must be bent into a loop. The TE011 mode is excited by electric coupling. Once the proper insertion depth is found, it is necessary to clamp down on the cable so that it does not move. This is achieved by a small screw drilled into the side of the lid (see figure 4-2)

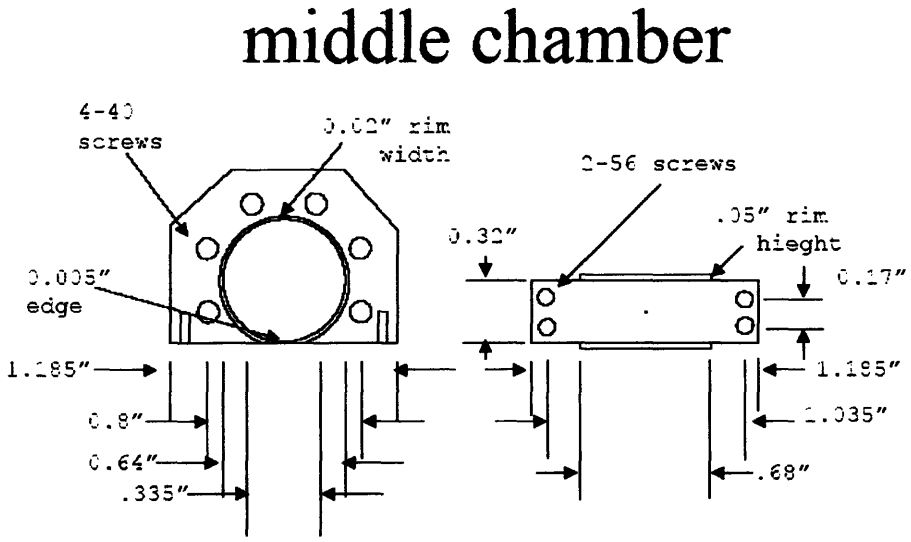

Figure 4-1: design of cavity body with measurement specifications.

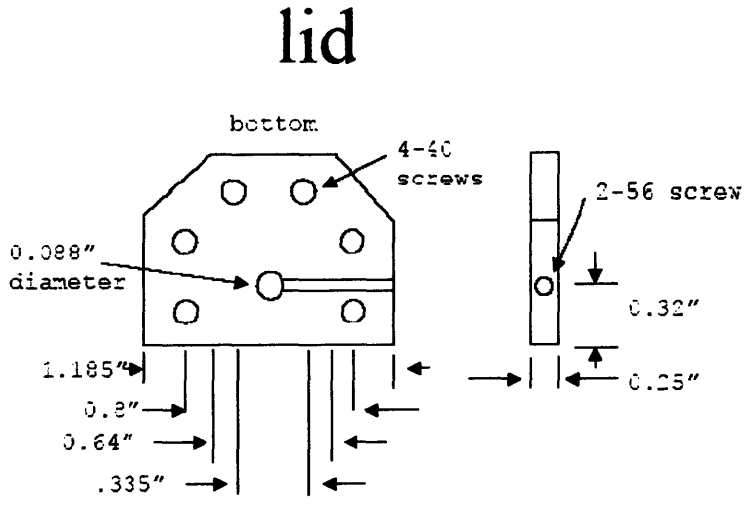

Figure 4-2: design of cavity lid. only the top lid has a hole intended for the coupling coaxial cable.

Chapter 5

Experiment

5.1 Testing the Cavities

Table 5.1 summarizes all of the experiments performed in testing the two cavities. Cavity A (designed for the TM010 mode) was tested at room temperature (RT), in a liquid nitrogen bath (LN2), and in an ST-100 cryostat designed to cool down to liquid helium (LHe) temperatures. Various lengths of coaxial cable were used to provide a better background oscillation. Several attempts were made to improve the seal between the body of the cavity and the lids, including physically tightening on the screws, replacing steal screws with brass screws, and finally drilling out the tapped holes to allow for through screws and bolts to clamp down on the cavity.

Cavity B (designed for the TE011 mode) was only tested at room temperature. During the first attempt there was a problem finding the precise mode. In order to break the degeneracy with the TM111 mode we placed tape around the rim of the lid. This would stop the flow of current between the lid and the cavity body, which is not needed for the TE011 mode. This technique made it very easy to isolate the correct reflection dip.

Table 5.1: Summary of Experiments

	Mode	Temp	Coax	Experiment	Freq. [GHz]	Q factor
1	TM010	RT	Cu, 8.8 inch	Before gold plating	14.065	2000
2	TM010	RT	Cu, 8.8 inch	After gold plating	14.050	1350-1450
3	TM010	RT	Cu, 6.0 inch	New coax	14.066	1700
4	TM010	RT	Cu, 6.0 inch	After tightening screws	14.086	3700-4400
5	TM010	RT	Cu, 55 inch	Long coax	14.083	3000
6	TM010	RT	Cu, 55 inch	Over coupled	14.085	3300
7	TM010	RT	Cu, 55 inch	Under coupled	14.091	3300
8	TM010	RT	Cu, 55 inch	New day	14.078	2500
9	TM010	LN2	Cu, 55 inch	Dipped in LN2	13.731	2200
10	TM010	RT	Cu, 55 inch	Switched to brass screws	14.094	3300
11	TM010	LHe	SS, 13 inch	Cooldown in ST-100	14.003	2450
12	TM010	LHe	SS, 13 inch	Through hole screws	14.147	3500
13	TM010	LHe	SS, 13 inch	New day	14.145	3100
15	TE011	RT	Cu, 42 inch	Broke contact with lids	15.105	4200

5.1.1 Equipment

The cavities were tested using a scalar network analyzer. A reflection bridge was placed at the output of the analyzer. This device isolates the waves that are sent to the cavity from those that are reflected back. The cryostat used was an ST-100.

5.2 Data Analysis

5.2.1 Fitting Parameters

The reflection data was analyzed using a fitting procedure written by Sami Amasha. The data is plotted on a logarithmical scale and must be fit for two important pieces, the background oscillation and the minima that come from finding a resonant mode of the cavity. There are 8 parameters to the fit:

Gamma

Gamma represents the reflection coefficient of the wave that is returned from the first reflection point. This wave forms interference with the wave that gets sent down the coax to the cavity and back again.

$$\Gamma_{rb} = \frac{Z_L - Z_0}{Z_L + Z_0} \tag{5.1}$$

T2

This is the overall phase factor for the interference oscillations.

D

This is the length of the coax. This parameter gives the period of the interference. Figure 5-4 shows the result of changing the length of the coax. Notice that the period of the oscillation changes from 0.5 GHz for a 6 inch coax to 0.06 GHz for a 55 inch coax.

offset

This is given by the power of the incoming signal. Because the data is plotted on a logarithmic scale, increasing or decreasing the power results in a vertical offset of the interference signal.

Coaxial Attenuation

This is given by the material properties of the coax being used. Table 5.2 gives the constants for the following equation for the two types of cables used to test the cavities, Stainless Steel and copper.

The power lost due to attenuation in a cable is given by the following:[1]

$$\texttt{Power lost}[-dBm] = [\alpha(f_0)^{\beta}] \times 2L \tag{5.2}$$

[1]Note that this is not an empiracle formula, it is mearly a fit to experimental data performed for the two types of coaxial cables

Table 5.2: Attenuation Constants

	SS	Cu
α	1.261	0.19
β	0.506	0.55

This power is given in units of debye per milliwatt. Here P stands for power in milliwatts and A stands for field amplitude.

$$Powerlost[-dBm] = 10log(\frac{P}{P_0}) = 20log(\frac{A}{A_0}) \tag{5.3}$$

$$attot = \frac{A}{A_0} = 10^{[-dBm/20]} \tag{5.4}$$

Q

The Q of the cavity results in the bandwidth of the reflection dip. See section 1.2 for details. Note that for Figures 5.2 and 5.5 the Q was improved by improving the contact between the lids and the body of the cavity.

Resonant frequency f_0

This occurs at the minimum of the reflection dip. Notice the change in resonant frequency when the screws are tightened in the experiment for Figure 5-2 and when the cavity is cooled in Figure 5-5. This can be understood because the dimensions of the cavity are changing slightly and the resonant frequency is given by Eq. (?).

Coupling

This is a measure of the efficiency of transmitting power into the cavity. If a cavity is over or undercoupled, it will have a loaded impedance. At perfect coupling the impedance will be perfectly matched. Coupling to the cavity can be modeled like a transformer. At a resonance frequency the impedance of cavity is purely real, however, it is not necessarily matched to the 50Ω impedance of the coax. If the resistance, R,

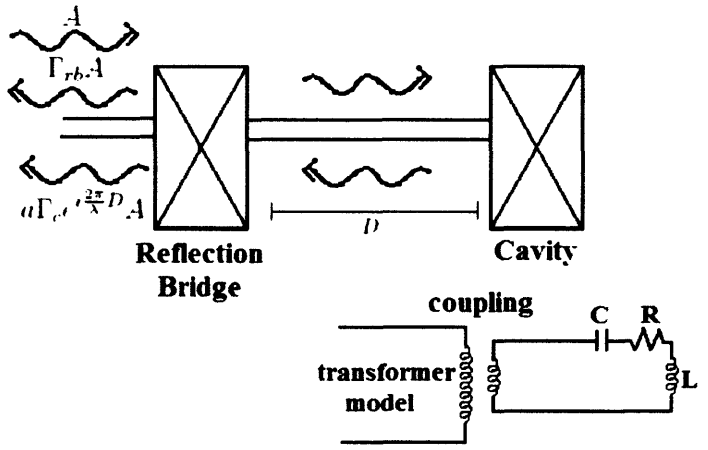

Figure 5-1: Difference in Q factor after tightening on screws

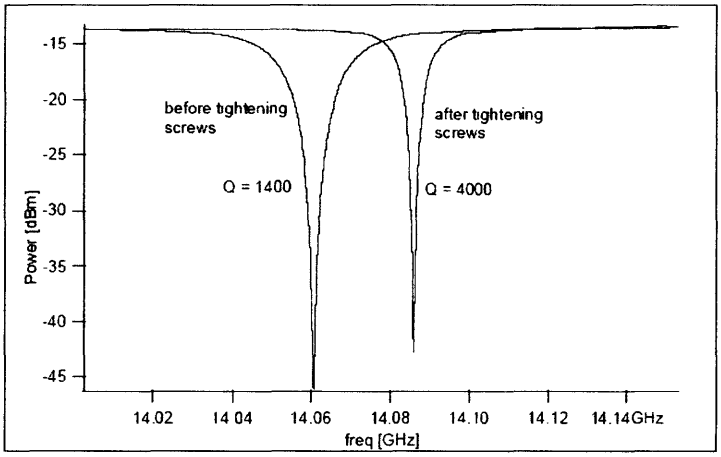

Figure 5-2: Difference in Q factor after tightening on screws

of the cavity after it is transformed by the cavity is given by $\frac{50\Omega}{n^2}$, where n is the coupling factor, then,

$$\Gamma_C = \frac{R - 50\Omega}{R + 50\Omega} = \frac{\frac{1}{n^2} - 1}{\frac{1}{n^2} + 1} \tag{5.5}$$

At perfect coupling, n = 1 and there is no reflection from the cavity.

5.2.2 Graphs

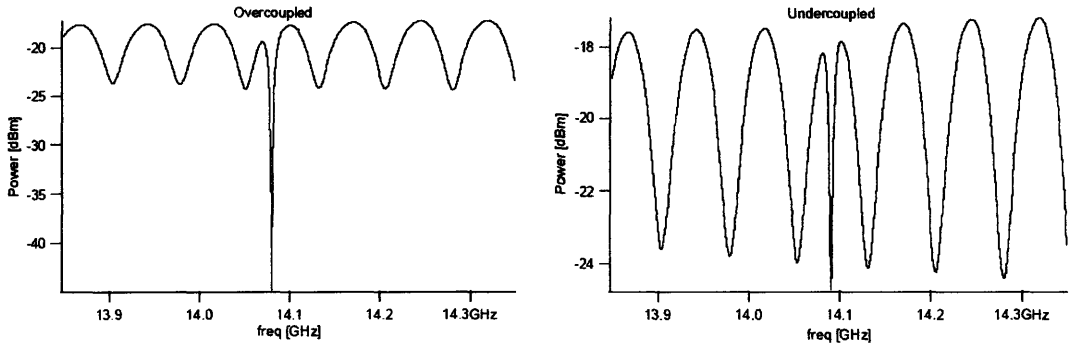

Figure 5-3: **Overcoupled and Undercoupled examples** Both fits give the same value for the Q factor but the depth of the reflection is different

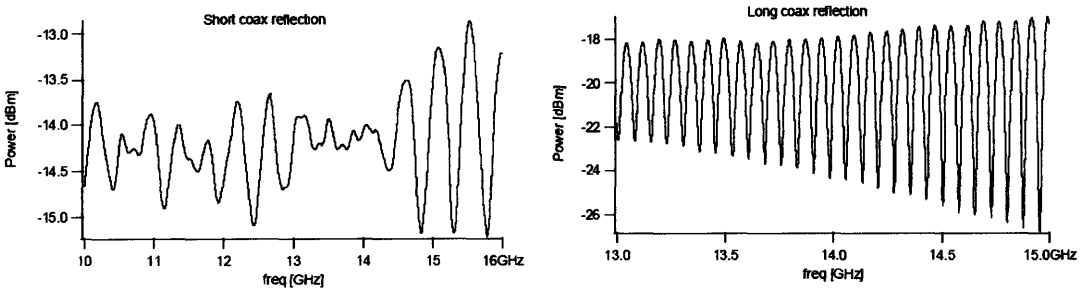

Figure 5-4: Difference in interference oscillation from short and long coax

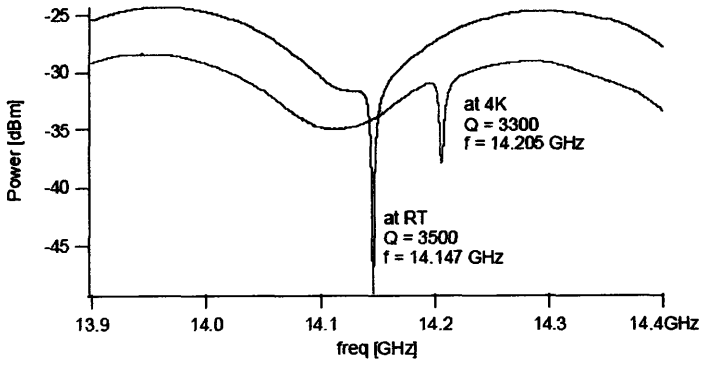

Figure 5-5: **Cooldown of cavity A** We were unable to improve the Q by cooling down, as would be expected

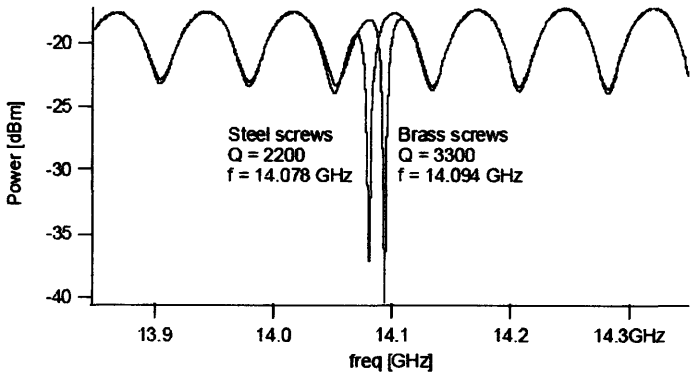

Figure 5-6: Improvement made be switching from steel screws to brass screws.

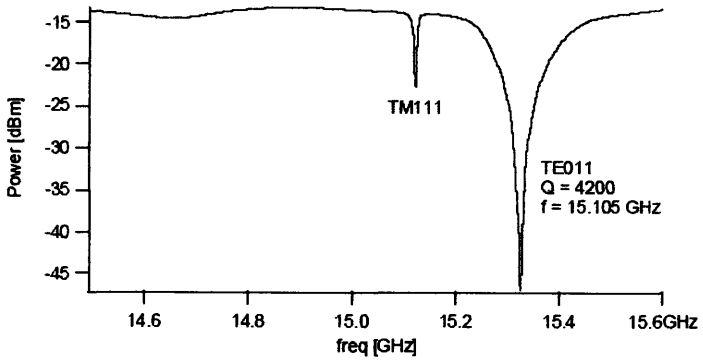

Figure 5-7: TM111 mode is nearly eliminated by breaking electrical contact between the lids and body of the cavity.

Chapter 6

Discussion

6.1 Results

Two cylindrical cavities were built, and both achieved Q's that were higher than the current rectangular cavity. The highest Q achieved was for TE011 mode with a value of 4200, this is much lower than the theoretically expected value of 20,000. This testing was only possible when we broke the contact between the body of the cavity and the lids because this eliminates the degeneracy with the TM111 mode. We have no idea why the Q was so low, and why it could not be improved at lower temperatures. The TE011 mode is impractical for our purposes for several reasons. First of all it is too large to fit in the cryostat. Secondly, because it did not have a Q that was as high as expected, field calculations show that the ratio of the useful magnetic field magnitude squared over the power lost is smaller than for the other cavities.

6.2 Suggestions for Future Designs

Wallace and Sillsby [7] describe a method of producing microstrip resonators for ESR measurements on silicon MOSFETs. They report that microstrips have from 3 to 10 times the sensity to 2D systems as waveguide cavities, while needing only about $\frac{1}{20}$th the sample area. They claim that their resonators are relatively immune to

vibrational noise and that for the same magnetic field, the microstrips require $\frac{1}{13}$ the incident power of a 3D cavity. Finally they say that the Q of their microstrip resonators improves by a factor of 5 at low temperatures whereas waveguide cavities can only improve by something like a factor of 2.

Bibliography

[1] Kastner, M. A., "Artificial Atoms." Physics Today 46(1):24 (1993)

[2] L. P. Kouwenhoven et al., *Electron Transport in Quantum Dots.*(ed) L. L. Sohn, L. P. Kouwenhoven and G. Schoen, NATO ASI Series E 345, p. 105 (1997).

[3] J. E. Wertz and J. R. Bolton, *Electron Spin Resonance.* Chapman and Hall, (1986).

[4] C. P. Poole, *Electron Spin Resonance.* Interscience Publishers, (1967).

[5] D. M. Pozar, *Microwave Engineering, 2nd Ed.* John Wiley and Sons, Inc., (1998).

[6] C. Kittel *Introduction to Solid State Physics, 8th Ed.* John Wiley and Sons, Inc., (2005).

[7] W. J. Wallace and R. H. Silsbee *Microstrip resonators for Electron-Spin Resonance.* Rev. Sci. Instrum. 62 (7) (1991).